Performance of the site-adapted CAMS database and locally adjusted cloud index models for estimating global solar horizontal irradiation over the Pampa Húmeda

A. Laguarda[a], G. Giacosa[a], R. Alonso-Suárez[a,*], G. Abal[a,b]

[a] *Laboratorio de Energía Solar, Instituto de Física, Facultad de Ingeniería, J. H. y Reissig 565, Montevideo, Uruguay*
[b] *Laboratorio de Energía Solar, Centro Regional Universitario Litoral Norte, Av. L. Batlle Berres km 508, Salto, Uruguay*

Abstract

CAMS provides global solar radiation estimates for clear-sky (McClear model) and all-sky (Heliosat-4 method) conditions, the latter based on MSG satellite information. A performance assessment of these estimates (with site-adaptation and spatial smoothing) is done, using hourly data from 10 sites in the Pampa Húmeda region of South America. Two locally adjusted Cloud Index Models (CIM) using GOES-East satellite information are also evaluated. One of them (CIM-ESRA) is based on the ESRA clear-sky model and the other (CIM-McClear) on the McClear clear-sky model. Under clear-sky conditions, the site-adapted McClear is found to perform best with a relative root mean square deviation (rRMSD) of 2.8%. However, in the presence of clouds in the real atmosphere, the model tends to provide lower clear-sky estimates than the ESRA model which, in our implementation, is only sensitive to average atmospheric trends. Under all-sky conditions, both CIMs show a small but consistent underestimation of −1.1% in the region and perform significantly better than the site-adapted Heliosat-4, with rRMSDs of 12.1% (CIM-McClear), 12.5% (CIM-ESRA) and 16.8% (site-adapted Heliosat-4). This performance difference is not a statement about the relative quality of the models, since it can be explained by the difference in satellite view angle (significantly higher for the MSG satellite than for the GOES-East satellite). The performance downgrade due to using MSG satellite images out of their recommended area is quantified. Both CIMs, based on using GOES-East imagery, provide accurate solar irradiation estimates over this region and can be extended to other areas of Latin America.

Keywords: Solar resource assessment, GHI, CAMS, satellite view angle, GOES satellite, hybrid models.

1. Introduction

The uncertainty of solar resource assessment is one of the main factors affecting the financial risk evaluation of large scale solar energy projects. This assessment ideally requires long-term, controlled quality, solar irradiation ground data for the project's site. Since this information is not usually available for a given project location, irradiation estimates based on geostationary satellite images are frequently used. These images provide the temporal and spatial resolution required for modeling a highly variable phenomena like ground level solar irradiation. The general idea is to quantify cloudiness using satellite information and use it to attenuate the clear-sky irradiation. Different models exist for this purpose (Perez et al., 2002; Ceballos et al., 2004; Rigollier et al., 2004; Cebecauer et al., 2010; Alonso-Suárez et al., 2012; Qu et al., 2017).

This work focuses on models for estimating ground-level solar global horizontal irradiation (GHI) from satellite information, working at the hourly time scale. Typical biases for hourly GHI satellite-derived estimates are within ±3.5% of the ground measurement's average (Perez et al., 2013), excluding special cases such as tropical regions, polluted areas, high latitude areas with snow, mountains or complex island sites, where higher biases can occur. Typical dispersion for hourly estimates (as quantified by the relative root mean square deviation or RMSD) for arid and semi-arid climates is in the range 7-20% and, for areas with more complex cloud dynamics, between 15-30% (Perez et al., 2013). Uncertainty can be reduced by spatial smoothing or site-adaptation techniques, the latter by post-processing the estimates using good-quality ground measurements (Polo et al., 2016).

Models for solar satellite-based estimation can be classified as empirical (Tarpley, 1979; Justus et al., 1986; Cano et al., 1986; Alonso-Suárez et al., 2012), physical (Ceballos et al., 2004; Qu et al., 2017) and hybrid (or semi-empirical) models (Perez et al., 2002; Rigollier et al., 2004; Cebecauer et al., 2010). Empirical models rely on parametrizations between solar irradiation and other variables (i.e. satellite-derived cloudiness, solar zenith angle) with a set of parameters that are adjusted from ground measurements. Physical models attempt to model in detail the radiative transfer of solar irradiance through the atmosphere. The Heliosat-4 method (Qu et al., 2017) is a recent example of a successful physical model based on Meteosat Second Generation (MSG) satellite images and radiative transfer

*Corresp. author: R. Alonso-Suarez, r.alonso.suarez@gmail.com

calculations. Hybrid models have an underlying physical structure with a few adjustable parameters. Both physical and hybrid models are potentially accurate provided the required information is available with sufficient quality. However, this information (i.e. aerosol optical depth, water vapor content, cloud type and phase, among others) is not always available with sufficient accuracy and spatial/temporal resolution. On the other hand, empirical models require high quality ground measurements of adequate length to adjust their parameters and their estimates cannot be extrapolated to other regions. Hybrid models provide a trade-off between empirical and physical models. A common hybrid model approach is to use a physical clear-sky model modulated by a satellite-derived cloud index to generate solar irradiation estimates under all-sky conditions. These models are collectively known as CIM (Cloud Index Methods). The SUNY model (Perez et al., 2002) and the early Heliosat models, Heliosat-1 (Beyer et al., 1996) and Heliosat-2 (Rigollier et al., 2004) are well known examples of this kind.

Another satellite-based model (of the empirical type) named BD-JPT, as it evolved from an original formulation by Justus, Paris and Tarpley (Justus et al., 1986), has been recently evaluated for the same region considered in this work (Alonso-Suárez et al., 2012). This model has been locally adjusted to ground data and used as a basis for the solar resource distribution map in Uruguay (Alonso-Suárez et al., 2014). In Alonso-Suárez et al. (2012), both the original JPT model and the improved brightness-dependent version (BD-JPT) have been evaluated for this region and showed interesting results: a relative RMSD of 13% at the hourly level with negligible bias was found. These models were implemented with the same GOES-East satellite information used in this work for locally adjusted CIMs, in particular, using the same spatial averaging procedure described in Subsection 3.2.4.

This work provides, among other contributions summarized at the end of this Section, a first representative assessment for the Pampa Húmeda region (South East part of South America) of the Heliosat-4 method (Qu et al., 2017). The clear-sky part of this method, known as the McClear model (Lefèvre et al., 2013), is based on a parametrization of the libRadtran libraries output (Mayer & Kylling, 2005). McClear uses atmospheric information from the CAMS (Copernicus Atmosphere Monitoring Service) and ground albedo from the sun-synchronous orbiting MODIS satellite (Moderate Resolution Imaging Spectroradiometer) to estimate clear-sky irradiation. These clear-sky estimates are combined with the McCloud model to produce the Heliosat-4 all-sky irradiation estimates. Cloud information and properties are derived from multiple spectral channels of the MSG satellite using the APOLLO/SEV algorithm (WDC, 2015). Here, the performance of this method based on the MSG satellite is compared against two locally adjusted hybrid CIMs which use cloud information derived from GOES-East satellite images. One of these CIMs is based on the ESRA (European Solar Radiation Atlas) clear-sky model (Rigollier et al., 2004) and the other is based on the McClear model. The performance comparison between a spatially smoothed site-adapted model based on MSG images and two locally-adjusted models based on GOES-East images helps to quantify the impact of the different viewing angles with which both satellites see the area of interest and emphasizes the importance of selecting the most adequate satellite information for each region.

Clear-sky models are important as a basis for CIMs and can be used to provide reliable upper bounds for automated quality assessment of ground data or to compute the clear-sky index required by several applications, such as variability assessment or solar resource forecasting. Therefore, the performance of the two clear-sky models used in this work (ESRA and McClear) is also evaluated. These models differ markedly in their description of the atmosphere. While McClear captures the daily and intra-day atmospheric variability, ESRA has a single parameter which, in our implementation, describes average atmospheric information, as explained in Subsection 3.3. This allow us to show a significant difference in the behavior of the clear-sky estimates whether the actual real atmosphere is clear-sky or cloudy.

The main contributions of this work can be summarized as follows:

- Compares the performance of satellite-based models for all-sky hourly irradiation estimate based on different geostationary satellite information and quantifies the impact of using satellite estimates out of their recommended area (i.e. satellite zenith angle larger than 60°).

- Compares two clear-sky models that differ in their capability for modelling the short-term atmospheric variability, in particular, by using water vapour as an input. For instance, it is found that when clouds are present in the atmosphere, modelling the short-term variability provides lower clear-sky estimates than using average atmospheric information. The rationale is that the presence of clouds correlates with higher water vapour contents in the atmosphere and this results in lower clear-sky estimates.

- Provides a first representative performance assessment of the Heliosat-4 method and locally adjusted CIMs for the Pampa Húmeda area, including the gain quantification of a simple site-adaptation procedure applied to the Heliosat-4 estimates.

- Quantifies the effect of the satellite information spatial smoothing in the region to reduce the uncertainty of hourly GHI estimates.

The article is organized as follows: Section 2 describes the satellite images, the ground data and the CAMS products used in this work, including a short discussion on the typical view angles from each satellite. In Section 3 the locally implemented models and their local-adaptations are discussed. This Section also describes the spatial smoothing procedure (applied to ensure that both satellite data sets have the same spatial averaging required for a fair comparison). In Section 4 the performance assessment of these models is done and discussed. Finally, our conclusions are summarized in Section 5.

2. Data

The area of interest in this work is the part of south-eastern South America known as Pampa Húmeda, within latitudes 28°S and 36°S. As shown in Figure 1, it includes all the territory of Uruguay and parts of Argentina and southern Brazil. It is geographically homogeneous (mostly plain grasslands) with temperate climate and no important elevations. Although temperatures in winter can drop a few degrees below freezing point, snow episodes are rare. It is classified in the updated Köppen-Geiger climate classification (Peel et al., 2007) mostly as Cfa (temperate, without dry season, hot summers) with the exception of two small coastal regions dominated by the influence of the Atlantic Ocean and classified as Cfb (temperate, without dry season, warm summers).

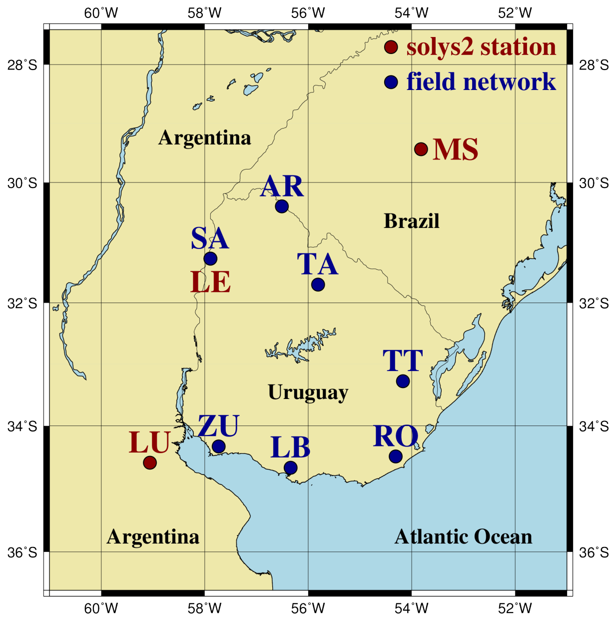

Figure 1: Location of the ground measurements stations.

2.1. Ground measurements

Ten series of GHI ground measurements are considered in this work. They belong to two groups, based on the quality of the instruments and the declared maintenance schedule at each site. The first group is composed by three ground stations located in Uruguay, Argentina and Brazil, whose equipment and procedures comply with BSRN requirements (McArthur, 2005): (i) the Solar Energy Laboratory experimental research facility (LE) in the north-western part of Uruguay (LES, http://les.edu.uy), (ii) the São Martinho da Serra station (MS), formally a BSRN site, and (iii) the Luján station (LU) located 50 km from Buenos Aires (Argentina) at a specialized research laboratory of the Luján National University (GERSolar, http://www.gersol.unlu.edu.ar/). At these sites, GHI is measured with ventilated secondary standard pyranometers and direct and diffuse irradiance are measured using precision solar trackers. Data are recorded as 1-min averages of several measurements. The LE instruments are calibrated every two years against a secondary standard (Kipp & Zonen CMP22) kept in storage and with traceability to the World Radiometric Reference (WRR). At the LU site, instruments are compared periodically against a Kendall absolute cavity radiometer, calibrated in 2018 with traceability to the WRR, which is stored and used sporadically as a reference. The São Martinho da Serra station (code MS) is part of the Brazilian SONDA network (http://sonda.ccst.inpe.br/), installed and administrated by the National Institute for Space Research (INPE, Brazil). This network meets the quality criteria established by World Meteorological Organization (WMO) and was specifically designed to record high-quality meteorological data in different climatic regions of Brazil (Dias da Silva et al., 2014). Cleaning and visual inspection at these sites is performed on a daily basis. Based on our experience, the assigned (P95) global uncertainty for hourly GHI measurements from these sites (LE, LU, SM) is 3% of the average.

The second group is composed with data from seven sites of Uruguay's LES solar radiation network, where spectrally flat class A or B (according to the new ISO 9060:2018 standard) Kipp & Zonen pyranometers are used to measure GHI, among other variables. All these sites are located either at manned meteorological stations or agronomic experimental facilities, and the pyranometers are cleaned and inspected at least on a weekly basis. These instruments are calibrated at LES at most every two years against the Kipp & Zonen CMP22 secondary standard mentioned before. Hourly GHI data from these sites is assigned a typical (P95) global uncertainty of 5% of the average.

The location of these sites is provided in Table 1 and their geographical distribution is shown in Figure 1. The data time-period for each site is provided later in Table 2, jointly with the quality filtering summary. Only data sets with a minimum 2-year statistics and complete years (or years and a half) are considered to avoid introducing seasonality bias in the data.

2.2. Satellite images

The target area shown in Figure 1 is covered by two geostationary satellites: the GOES-East (operated by the National Oceanic and Atmospheric Administration, NOAA) and the MSG (operated by the European Organisation

	code	lat (°)	lon (°)	alt (m)
LES facility	LE	-31.28	-57.92	56
São Martinho da Serra	MS	-29.44	-53.82	489
Luján	LU	-34.59	-59.06	30
Canelones (Las Brujas)	LB	-34.67	-56.34	38
Treinta y Tres	TT	-33.28	-54.17	35
Salto	SA	-31.27	-57.89	47
Rocha	RO	-34.49	-54.31	20
Artigas	AR	-30.40	-56.51	136
Colonia (La Estanzuela)	ZU	-34.34	-57.69	70
Tacuarembó	TA	-31.71	-55.83	142

Table 1: Information of the ground measurement stations.

for the exploitation of Meteorological Satellites, EUMETSAT). Due to their positions in the geostationary orbit, they have different pixel sizes and view angles over the area. The GOES-East satellite pixel size is approximately 2 km, as expected over the region for the 1 km nadir spatial resolution of the former GOES12 and GOES13 satellites (Lockheed-Martin, 2019). On the other hand, the MSG satellite has a nadir spatial resolution of 3 km (Schroedter-Homscheidt et al., 2018) and the pixel size over the region is of approximately 7 km[1]. The satellites' zenith angles for the target region are approximately 40° and 70° for the GOES-East and MSG, respectively.

Cloud properties and irradiation estimates from satellite images with view angles above 60° are prone to higher errors mainly due to increased pixel size, parallax errors which produce apparent cloud displacement and the failure to fulfill the plane-parallel assumption (Johnson et al., 1994; Schroedter-Homscheidt et al., 2018). CAMS produces regular publicly available validation reports in which its irradiation products are compared to several quality ground sites. Figure 2, based on data from a recent validation report (Lefèvre, 2018), shows the dispersion of the Heliosat-4 estimates (as quantified by rRMSD) vs the satellite zenith angle z of the ground site. A clear threshold is apparent, just below 60°. Sites with $z < 55°$ have average rRMSD of about 11% while those with $z \geq 55°$ have rRMSD of about 25%. So, large viewing angles can affect seriously the accuracy of the irradiation estimates. The CAMS User Manual sets the recommended upper limit for view angle at 60°, while still providing the information for higher view angles (Schroedter-Homscheidt et al., 2018, Sec. 5.2).

Information from both satellites is considered in this work: cloudiness information for the CIMs is derived from GOES-East images, while the Heliosat-4 solar irradiation estimates are based on MSG images. GOES-East satellite images were downloaded from the NOAA CLASS (Comprehensive Large Array-data Stewardship System) website (https://www.class.noaa.gov/), where they are publicly available. Information from the MSG satellite is used here out of the recommended zone (satellite zenith angle above 60°) in order to quantify the impact of using such information for solar resource assessment in the region. The target area location in both satellites fields of view (FOV) is shown in Figure 3.

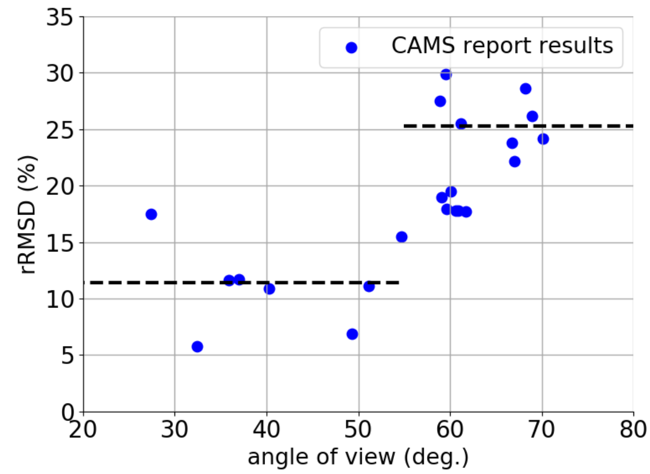

Figure 2: Dispersion (rRMSD) of Heliosat-4 GHI estimates vs view angle z for several sites. Data obtained from (Lefèvre, 2018). The dashed lines indicate average rRMSD for $z < 55°$ and $z \geq 55°$.

2.3. *CAMS products*

This Subsection briefly describes the CAMS products that are used in this work. The data was retrieved from the CAMS Radiation Service at http://www.soda-pro.com/. These estimates are provided with a reliability flag and only the highest reliability estimates were used.

2.3.1. *McClear model*

As mentioned in the introduction, the McClear model produces clear-sky GHI estimates based on look-up tables (LUT) of the libRadtran Radiative Transfer Model (RTM) (Lefèvre et al., 2013; Mayer & Kylling, 2005), which in turn uses atmospheric information from satellite retrievals. Being based on LUT, the McClear model can be used operationally (i.e., in real time) since the substantial computational cost of the RTM calculations is avoided. McClear estimates are available at 1-minute intervals with worldwide coverage while the model inputs are typically available every three hours with a spatial resolution between 50-150 km. Using interpolation techniques, the SoDa website provides estimates for any latitude-longitude combination at 1-minute time resolution and above.

In Lefèvre et al. (2013), McClear clear-sky GHI estimates were compared to 1-minute clear-sky measurements from eleven BSRN stations covering different climates in America, Europe, Asia, and Oceania. Mean biases between −1% and +3% and mean rRMSD in the range 3-5% were obtained (in both cases expressed relative to mean observed irradiance). This model has also been assessed at the 10-minute level against data from seven sites in United Arab Emirates (Eissa et al., 2015b), where the atmosphere is mostly free of clouds but can have high turbidity. The

[1] For more information see http://www.soda-pro.com

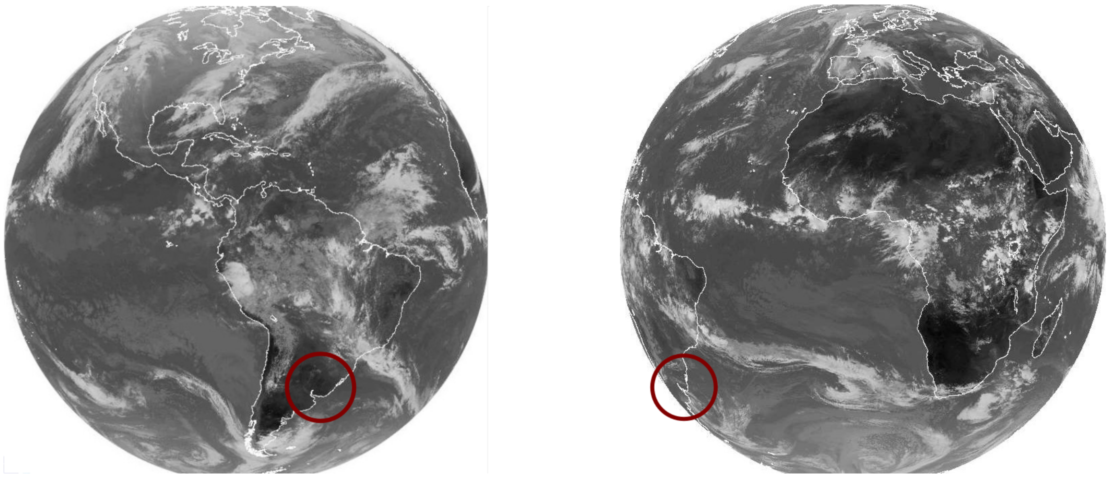

(a) GOES-East satellite FOV. Position: 75°W.   (b) MSG satellite FOV. Position: 0°.

Figure 3: Satellites' field of view (FOV) identifying in red the area under study. Infrared images are used only for visualization purpose.

rMBD was in the range -1% and $+6\%$ and the rRMSD was between 4-8%. In a similar climate, using 1-minute measurements from three sites in Israel, McClear had relative biases between zero and $+4\%$ and a rRMSD of 4% (Lefevre & Wald, 2016). With the exception of Lefèvre et al. (2013), which considers one site in Brasilia, Brazil (with different climate and distant more than 2000 km from the region of interest in this work), there are no other validations of the McClear model in South America.

2.3.2. *Heliosat-4 method*

The Heliosat-4 method (Qu et al., 2017) estimates GHI and its components under all-sky conditions. It is based on the McClear model and a second LUT model, the McCloud model, also based on RTD calculations. McCloud estimates the attenuation of Shortwave Solar Irradiation (SSI) due to cloudiness using a clear-sky index based on an abacus with four inputs: ground albedo, cloud optical depth, cloud coverage and cloud type. Cloud information is obtained from the APOLLO/SEV methodology, while ground albedo comes from MODIS. APOLLO/SEV is an adaptation of NOAA's APOLLO algorithm (AVHRR Processing scheme Over cLouds, Land and Ocean; Kriebel et al. (1989, 2003)) for the SEVIRI (Spinning Enhanced Visible and Infrared Imager) instrument. This procedure discriminates each pixel in different categories of cloud coverage before deriving its physical properties. The model considers four categories of cloud type and assigns one of these types to each covered pixel. The optical depth is assigned to each cloudy pixel depending on the multi-spectral APOLLO/SEV procedure that provides this information only for fully cloudy pixels. Interpolation techniques are used for pixels in other categories. Based on this input information, for each abacus node a clear-sky index is retrieved, and then used to calculate GHI using a clear-sky libRadtran run over a standard atmosphere. More details of this sophisticated model can be found in Qu (2013).

The Heliosat-4 method was first validated against measurements from 13 BSRN stations on a 15-minute basis in Qu et al. (2017). Ten of these sites are located in Europe (including one in the Canary Islands), while the rest are in Israel, South Africa and Algeria. This assessment of the model showed rRMSD values between 15-20% in desert and mediterranean climates and between 26-43% in rainy climates with mild winters. The automatic validation reports provided by CAMS at the hourly level (www.soda-pro.com/web-services/validation) using the period 2014-2018, include two sites in the target region of this work. One is an urban site in Buenos Aires (Argentina) and the other is a coastal site in Florianopolis (Brazil). Neither of these sites is representative of the region under study. The former is located in a densely populated urban area where high atmospheric turbidity is frequent. The latter is located in an Atlantic coast island with a climate dominated by the ocean and is more than 1000 km away from the closest site used in this work. Performance in these two sites shows rMBDs of -5% and 0% and rRMSDs of 25% and 28%, respectively. Both sites have relatively high viewing angles outside the recommended range, 73° for Buenos Aires and 62° for Florianopolis. In Toravere, Estonia, a region with similar satellite view angle (70°), the evaluation shows a positive bias of $+3\%$ and an rRMSD of 28%. On the other hand, in Carpentras, France, with zenith angle 51° the rMBD $+2\%$ and the rRMSD is only 15%. Another case is Tamanrasset, Algeria, a desertic location near the satellite nadir (zenith angle 27°), where the performance is -5% rMBD and 15% rRMSD. The rRMSD for these and other sites are included in the CAMS quarterly validation report and are plotted vs satellite zenith angle in Figure 2 to display the increase in rRMSD for sites beyond $z = 60°$.

3. Methodology

This Section is organized as follows. Subsection 3.1 presents the quality assessment and clear-sky selection procedures applied to the data sets. Subsection 3.2 describes the locally implemented models, ESRA model and both CIMs, including the cloud index calculation and the spatial smoothing applied to the satellite information to reduce the uncertainty of hourly estimates. This spatial smoothing procedure is also applied to the CAMS Heliosat-4 product, for a fair comparison, as explained at the end of Subsection 3.2.4. Finally, Subsection 3.3 describes the local adaptation procedures used for the different models and estimates. This includes the adjustment of locally implemented models and the site adaptation of CAMS products, for fair comparison.

3.1. Pre-processing of data

Hourly horizontal irradiation was calculated for each site from the original one-minute ground measurements. Hours with more than 10-minute gaps were discarded. The following quality-control filters were applied to the daylight hourly GHI measurements:

(i) Minimum solar elevation: $\alpha_s > 7^o$; in order to avoid data affected by large cosine errors.

(ii) Maximum irradiation: $\text{GHI} < \text{GHI}^*_{\text{csk}}$; the ESRA clear-sky model (Subsection 3.2.1) was used with a low Linke turbidity factor $T_L = 2$ to compute $\text{GHI}^*_{\text{csk}}$ as an upper bound for GHI. This value of T_L is sufficiently low (see the average T_L cycle shown in Figure 5) for this purpose and it has been previously used in this region to generate an upper bound for hourly GHI (Abal et al., 2017).

(iii) Modified clearness index bounds: $0 < k'_T < 0.85$; the modified clearness index, k'_T, is defined in Perez et al. (1990).

(iv) Coincident pairs of GHI and GOES-East satellite information. The samples discarded at this stage are mainly determined by the GOES-East satellite availability, as discussed below.

(v) Coincident pairs of GHI and Heliosat-4 estimates. As mentioned, only Heliosat-4 estimates flagged with the highest reliability are considered.

GOES-East image availability for South America was irregular before the year 2018, when the new GOES-R started operations at the GOES-East position. For the period 1997-2017, these images are normally available at a rate of two per hour. However, hourly or tri-hourly gaps result for South America when the GOES-East satellite was placed under Rapid Scan Operation mode for specific areas. The hourly satellite information was obtained by linear interpolation of the satellite time series under the restriction of not interpolating across gaps larger than three hours.

The filtering results for each site are summarized in Table 2, where filters (ii) and (iii) are grouped in a single column for brevity. It describes the filters sequentially applied to the initial data set (daylight values), so that each discard percentage refers to the previous column and the number of records that passed all previous filters is informed at each stage. The last two columns indicate the final hourly records for all-sky and clear-sky conditions, respectively. After this filtering procedure, a set of 160298 hourly GHI records are available for the all-sky model assessment.

The selection of the clear-sky subset was based on the procedure proposed by Remund et al. (2003). This algorithm is based on five consecutive filters applied to hourly data, but the main criterion is to impose a lower threshold of 0.7 on the modified clearness index, k'_t (Perez et al., 1990). We added an extra filter to this procedure imposing a bound on daily variability: if the standard deviation of the k'_t series within a day was over 0.05, the whole day was discarded. The threshold of 0.05 was heuristically determined to ensure that only clear-sky records were selected, since any contamination by partly cloudy samples would artificially affect the clear-sky models performance assessment. The amount of clear-sky hours selected for each site is indicated in the last column of Table 2. Considering all sites, 34050 hourly clear-sky samples were selected.

3.2. Locally implemented models

3.2.1. ESRA model

The ESRA clear-sky model was developed in the framework of the European Solar Radiation Atlas (Rigollier et al., 2000) and used with Meteosat images as part of the Heliosat-2 method for SSI modeling (Rigollier et al., 2004). It estimates direct normal irradiance (DNI) and diffuse horizontal irradiance (DHI) under clear-sky conditions. The GHI estimate is obtained from $\text{GHI} = \text{DNI} \times \cos\theta_z + \text{DHI}$. The single input in this model is the Linke Turbidity factor, T_L, for air mass 2. It is usually interpreted as the number of clean, dry atmospheres (i.e. with no clouds, water vapor or aerosols) which would produce the same attenuation effect on GHI as the real cloudless atmosphere. Thus, T_L includes in one effective parameter the information on water vapor density and aerosol contents of the real atmosphere (Linke, 1922; Ineichen & Perez, 2002). Given its simplicity and the fact that it may provide accurate estimations if the T_L values are locally obtained with sufficient time resolution (Gueymard, 2012), the ESRA model is a frequent choice to model clear-sky irradiation. Here, the T_L cycles have been derived on an monthly basis from the GHI measurements, as discussed in Subsection 3.3.

ESRA model performance has been analyzed in several studies (Gueymard, 2012; Engerer & Mills, 2015; Ineichen, 2016; Antonanzas-Torres et al., 2019; Sun et al., 2019) that consider different climates around the world. This model

site	period	daylight hours	(i) solar altitude disc.	(i) solar altitude hours	(ii) & (iii) bounds disc.	(ii) & (iii) bounds hours	(iv) GOES images disc. (%)	(iv) GOES images hours	(v) CAMS reliability disc.	(v) CAMS reliability hours	clear-sky hours
LE	01/15–12/17	12432	9.8%	11216	1.9%	11004	0.4%	10964	6.0%	10307	2783
MS	01/10–12/16	30199	9.0%	27493	2.3%	26854	1.8%	26367	6.9%	24553	5257
LU	01/10–12/13	17025	10.7%	15195	3.0%	14741	3.1%	14283	9.5%	12925	3282
LB	06/10–12/17	28826	10.3%	25843	1.8%	25383	2.0%	24882	6.6%	23232	4931
TT	06/10–05/16	24705	9.8%	22294	3.0%	21629	2.2%	21153	7.1%	19652	2790
SA	06/10–12/14	19083	9.8%	17216	1.7%	16930	2.9%	16446	8.1%	15122	4412
RO	06/11–12/17	27120	9.6%	24514	2.8%	23831	2.0%	23351	6.0%	21940	3329
AR	01/12–12/17	21955	9.0%	19970	2.3%	19509	1.1%	19290	6.3%	18071	4239
ZU	01/16–12/17	8686	10.6%	7766	1.6%	7645	0.5%	7605	5.2%	7206	1514
TA	01/16–12/17	8659	9.1%	7871	2.2%	7697	0.5%	7658	4.8%	7290	1513
total		**198690**	**9.7%**	**179378**	**2.3%**	**175223**	**1.8%**	**171999**	**6.8%**	**160298**	**34050**

Table 2: Quality check and data set description for each ground measurement site. The % discarded and the number of hours that pass each filter are informed. The last two columns indicate the all-sky and clear-sky hours used for model assessment.

usually is well ranked among other simple proposals and its uncertainty mostly depends on the quality of the T_L input data being used. Its validation in the Pampa Húmeda region has been scarce and comprises only one preliminary local study using five measurement sites in Uruguay (Laguarda & Abal, 2017) where a rMBD of −0.5% and a rRMSD of 4.5% were found for clear-sky hourly GHI estimation. Validations for similar climates (Cfa and Cfb in the Köppen-Geiger classification) are as follows. In Gueymard (2012) a rMBD of +4.3% and rRMSD of 4.9% was found for the ARM-SGP site (Oklahoma, USA) using 1-minute GHI measurements. In Engerer & Mills (2015) the ESRA model was evaluated at 14 sites using 1-minute GHI data from the Australian Bureau of Meteorology, four of which are in the relevant climate zones. For these, rMBDs between +2% and +9%, and rRMSDs between 3.7% and 8.0% were found. An exhaustive revision of 38 validation studies of clear-sky models performance, most of them including ESRA, can be found in Ruiz-Arias & Gueymard (2018). Overall, there is a considerable spread in the performance of the ESRA model, depending on climate and implementation details, and simplicity is one of its key features.

3.2.2. *Cloud Index Methods (CIM)*

As mentioned before, this family of SSI models has the common structure of a clear-sky model with a modulating factor that takes into account the effect of clouds. The clear-sky index, $\mathrm{GHI}/\mathrm{GHI}_{csk}$, can be modeled by a cloud attenuation factor, $F(C)$, which depends on the satellite-derived cloud index C defined in the following in Eq. (3). In this work, we use a simple linear function,

$$F(C) = a + b \times (1 - C), \tag{1}$$

where a and b are locally adjusted for each site. Then, GHI is computed from:

$$\mathrm{GHI} = \mathrm{GHI}_{csk} \times F(C). \tag{2}$$

In this work, Eqs. (1) and (2) are implemented using the two clear-sky models discussed before (ESRA and McClear) and the resulting CIMs are referred in what follows as CIM-ESRA and CIM-McClear, respectively. We emphasize that the a and b parameters in Eq. (1) are site and model-specific. The coefficients for CIMs in the region are part of the results of this work and are discussed in Subsection 3.3 on local adaptation (Table 3).

3.2.3. *Cloud index calculation*

The satellite-derived cloud index (Cano et al., 1986), C, is a dimensionless parameter in $[0, 1]$ that quantifies the amount of cloudiness. It is obtained from the Earth albedo (or planetary reflectance), ρ_p, by normalization with extreme values $\rho_{\min}$ and $\rho_{\max}$ associated with clear and overcast skies respectively,

$$C = \frac{\rho_p - \rho_{\min}}{\rho_{\max} - \rho_{\min}} \quad \text{for} \quad \rho_{\min} < \rho_p < \rho_{\max}. \tag{3}$$

Additionally, the constrains $C = 1$ for $\rho_p > \rho_{\max}$ and $C = 0$ for $\rho_p < \rho_{\min}$ are imposed. The parametrization proposed in Tarpley (1979) is used in this work to estimate the intra-day and seasonal variation of the background albedo. This parametrization models the background reflectance factor, $F_{Ro} = \rho_{po}/\cos\theta_z$, and needs to be adjusted for each pixel in the image using satellite clear-sky samples. These clear-sky samples are automatically selected from the pixel's satellite time-series by a robust iterative procedure described in Alonso-Suárez et al. (2012). This adjustment procedure can be updated on real time taking the past pixel samples, but for the sake of this work it was done only one time using the 2010-2017 satellite period. After the coefficients for each pixel (or site) are adjusted, whether on real-time or offline, the parametrization can be used to estimate the F_{Ro} time-series at hourly intervals. Then, the $\rho_{\min}$ time-series is calculated by setting $\rho_{\min} = \rho_{po} = F_{Ro}/\cos\theta_z$. A proper background albedo characterization is an important step in order to obtain useful cloud index information. For $\rho_{\max}$, a fixed constant value of 0.80 is chosen, since this value has been found to optimize the performance in the region of satellite-based models for GHI (Laguarda et al., 2018).

3.2.4. Spatial smoothing

In order to use satellite information at an hourly basis, the reflectance ρ_p obtained from GOES-East images has been spatially averaged in a 10 min $\times$ 10 min latitude-longitude cell centered at the site of interest. For this target region, this corresponds to cells of approximately 16 km $\times$ 18 km. This is equivalent to an ergodic hypothesis, where the spatial average of an instantaneous image within a cell is representative of the average conditions at the center of the cell within the hour. The cell size has been optimized to minimize the uncertainty of hourly satellite models. The rRMSD trend as a function of the cell size is shown in Figure 4, based on the CIM-McClear model. This curve is essentially the same as a similar one reported in Alonso-Suárez (2017), but using different ground stations, data time-span and satellite model. Hence, this curve can be considered characteristic for locally-adapted satellite based models in the target region. Inspection of Figure 4 shows that the minimum is shallow and essentially the same performance is obtained between 8 min and 12 min latitude-longitude spacing, which approximately correspond to cells with 12 km $\times$ 15 km and 18 km $\times$ 22 km area, respectively.

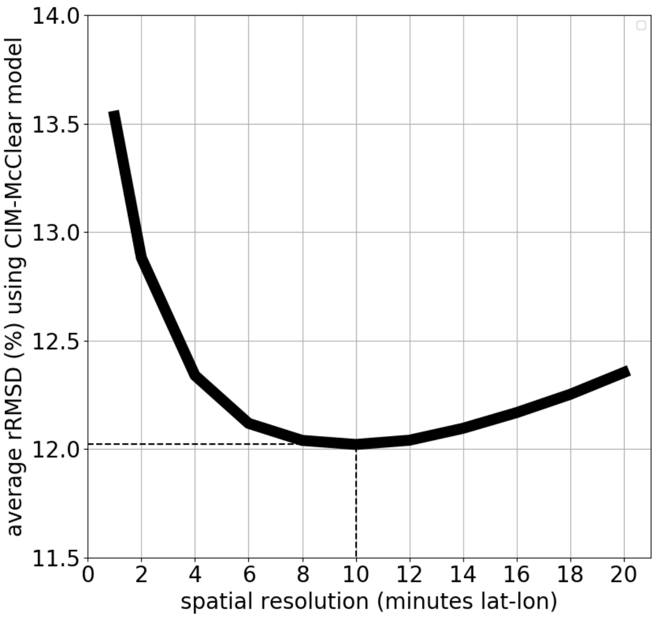

Figure 4: Local rRMSD curve as a function of the spatial smoothing.

The Heliosat-4 estimates are generated for single pixels without any spatial smoothing (pixel size is around 6-7 km, as discussed in Subsection 2.2). For fair comparison, the Heliosat-4 estimates were downloaded for each site in a grid of 3×3 pixels surrounding each location, accounting for a similar spatial averaging ($\simeq 21$ km $\times$ 21 km). The average of the nine time-series has been used as the model's estimates for each site.

3.3. Local adaptation

The aim of local adaptation is to reduce bias and, more generally, to improve model performance in a given homogeneous geographical area. It can be achieved either by locally adjusting the model's parameters or by site-adapting their estimates. Since the CIMs have locally adjusted parameters, for a fair comparison, the estimates available from CAMS for the McClear and Heliosat-4 models must be site-adapted.

A widely used site adaptation technique consists of a linear regression correction between the hourly model estimates and the ground data (Polo et al., 2016). This strategy is used in this work to site-adapt the estimates from both CAMS models. In Section 4 the results for McClear model and Heliosat-4 method are provided with and without site-adaptation, so the performance gain of the adaptation procedure can be observed.

CIMs, based on the site-adapted McClear or ESRA estimates, are locally adapted by adjusting their two parameters to ground data (a and b, see Eq. (1)) using a standard cross validation technique, where half of the data is randomly selected to train the model and the other half is used to evaluate its performance. The procedure is repeated 1000 times to ensure repeatability, and the ensemble average uncertainty and adjusted parameters are reported. In this context, it is worth pointing out that the cloud index calculation includes also an implicit local adaptation at each pixel, as the ground albedo (image background brightness) has been locally adjusted by modelling the F_{Ro} (and ρ_{min}) time series, as described in Subsection 2.2. The locally adjusted parameters for the CIMs are shown in Table 3 for each site. Both CIMs have similar values for a and b and there is a good agreement across sites. This is considered a sanity check for the proposals and the adjustment, as the region is mostly uniform in geography and climate. Thus, the average set of parameters can be used for the region without significantly affecting performance.

In the case of the ESRA clear-sky model, the local adjustment is made through the T_L values used as input. Yearly cycles of average T_L values are estimated for each site using its GHI data and the ESRA GHI clear-sky parametrization. These values were obtained from clear-sky samples of ground measurements by minimizing the statistical deviation between the model and the ground truth, as detailed in Laguarda & Abal (2016). The resulting average T_L cycles have a small spatial variation, as shown in Figure 5, where the spatially averaged yearly cycles for T_L are shown for two broad regions which correspond approximately to the areas of Figure 1 separated by latitude 33°S (North and South). Values for T_L are between 2.8 and 4.2, with higher values in the summer and lower values in winter.

This method captures seasonal effects and models the average trends in the local atmospheric turbidity and water vapor. However, it does not attempt to model its daily or hourly variability. In this way, the issue of using dif-

	CIM-McClear		CIM-ESRA	
site	a	b	a	b
LE	0.073	0.92	0.040	0.94
MS	0.076	0.91	0.053	0.92
LU	0.062	0.92	0.041	0.93
LB	0.068	0.91	0.044	0.93
TT	0.072	0.90	0.052	0.91
SA	0.055	0.93	0.031	0.94
RO	0.075	0.90	0.054	0.91
AR	0.076	0.91	0.048	0.92
ZU	0.070	0.91	0.045	0.92
TA	0.074	0.91	0.045	0.93
mean	**0.070**	**0.92**	**0.045**	**0.93**
σ	**9.7 %**	**1.0 %**	**15.6 %**	**1.2 %**

Table 3: Locally adjusted parameters of cloud index models (Eq. (1)). The last two rows show the weighted average and the standard deviation (P67) as a %.

ferent T_L formulae based on different quality satellite retrievals or atmospheric inputs is avoided.

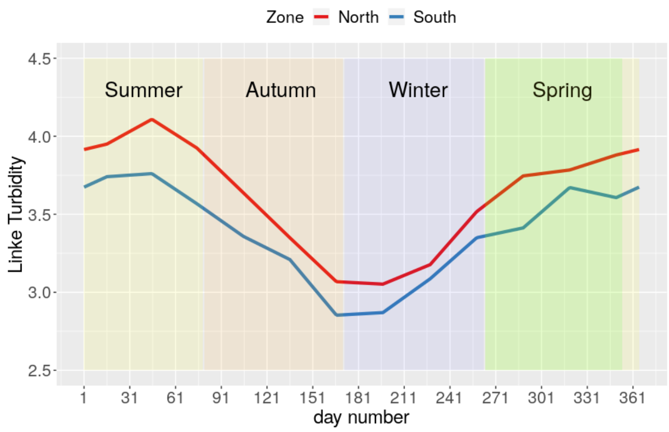

Figure 5: Daily cycles for T_L (no unit) obtained from clear-sky data in Laguarda & Abal (2016). The northern and southern zones are separated approximately by the 33°S latitude parallel (see Figure 1).

4. Results

4.1. Performance metrics

The performance assessment is done using three common indicators: the mean bias deviation (MBD), the root mean square deviation (RMSD) and the Kolmogorov-Smirnov integral (KSI). The first two measure the average bias and the average dispersion of the residuals, respectively. These are expressed in relative terms as a percentage of the measurement average (rMBD and rRMSD, respectively). The KSI is a statistical similarity index based on the distance between the probability distributions of the measurements and the estimates (Massey Jr., 1951; Espinar et al., 2009). A useful discussion and examples of use of these indicators can be found in Gueymard (2014).

Whenever average metrics over all sites are reported, the P95 uncertainty assigned to each ground measurement's data set is used to weight the averages, so that higher quality data will have more impact on the indicators. The weight for each site is calculated as $w_i = c/u_i^2$ with u_i the assigned relative uncertainty for measurements from site i. The set of weights is scaled by c to add up to unity, $c \times \sum_i 1/u_i^2 = 1$. This standard weighting procedure has been previously used in a similar context with good results (Abal et al., 2017).

4.2. Clear-sky models (McClear, ESRA)

The performance assessment for clear-sky models under cloudless conditions is shown for each site in Table 4, where the last column shows the (weighted) average indicators over all sites and the last row shows the ground measurement averages for the clear-sky hours under comparison. This information is provided to enable the reader to compute the absolute indicators, if needed.

Both models, whether locally-adapted or not, perform well and within the expected ranges at all sites, and the rRMSD indicators are similar to the P95 uncertainty assigned to the high quality ground data sets. The McClear estimates as provided by the CAMS platform (without site adaptation) show a small positive average bias of +1.4% with small but consistent overestimation at all sites. The rRMSD values range from 2.7% to 4.3% with an average of 3.2% while the average KSI is 8.9 $\mathrm{Wh/m^2}$. This non site-adapted model's performance is similar to that of the ESRA model with locally adjusted T_L values, which has an average rRMSD of 3.5%. However, the site variability is lower for the ESRA model, ranging from 3.2% to 3.8%. This model is essentially unbiased (its average bias is −0.1% and it is within ±0.3% across all sites). This results in a lower KSI metric than the original McClear estimates, with a site-averaged KSI of 5.0 $\mathrm{Wh/m^2}$.

The site-adapted McClear model provides the best performance: it is unbiased and consistently has the lowest rRMSD and KSI across all sites. The site-average rRMSD of the locally adapted McClear is 2.8%, ranging from 3.7% at the oceanic RO site and as low as 2.5% at the high quality LE site. Similarly, the average KSI is 1.9 $\mathrm{Wh/m^2}$, showing a superior performance also from a statistical similarity point of view. As mentioned, this model takes into account the atmospheric short-term variability, while the less sophisticated ESRA model only takes into account seasonal trends in atmospheric turbidity.

These indicators (low or negligible bias deviation and rRMSD in the range 3-4%) are not surprising from locally adjusted clear-sky models (Gueymard, 2012). Lower indicators (around 2%) have been reported for detailed models with high quality atmospheric information, such as the REST2 clear-sky model at particular locations (Gueymard, 2008). Taking into account the uncertainties of our hourly ground data set, the performance assessment of the clear-sky models cannot be made to those limits. A shorter 1-minute time scale and pyrheliometer data (accurate to 1%) would be required to further explore the performance limits of the McClear or other models, such as REST2, in this region. However, this is out of the scope of this work.

4.2.1. Clear-sky models under all-sky conditions

In several applications, such as CIMs or short-term forecasting, the output of a clear-sky model is used under non clear-sky conditions. Thus, it is relevant to investigate the output characteristics of clear-sky models under non clear-sky conditions.

Figure 6 reveals a relevant difference between the two clear-sky models estimates under non clear-sky conditions. Both panels show the hourly clear-sky estimates from each model as a function of the cosine of the solar zenith angle for all-sky conditions. The ground measurements (all-sky) are shown in the background in grey. As shown in Figure 6a, the estimates from the McClear model are affected by the actual sky condition, being lower when there are clouds in the real atmosphere (blue dots) than under real clear-sky conditions (green dots). This behavior is not observed in the ESRA model (Figure 6b) where the estimates under clear-sky and all-sky condition show the same characteristics.

In the presence of clouds, particularly under heavy overcast conditions, there is more water vapour in the atmosphere. Since the McClear model takes into account the

model	metric	LE	MS	LU	LB	TT	SA	RO	AR	ZU	TA	all sites
McClear	rMBD (%)	1.1	1.8	0.7	1.7	1.8	1.3	2.1	2.7	2.1	2.8	**1.4**
(original)	rRMSD (%)	2.7	3.4	3.0	3.6	3.8	3.1	4.3	4.1	3.6	4.0	**3.2**
	KSI (Wh/m^2)	6.8	11.5	4.6	10.3	10.5	7.9	13.3	17.3	13.3	17.6	**8.9**
McClear	rMBD (%)	0.0	0.0	0.0	0.0	0.0	0.0	0.0	0.0	0.0	0.0	**0.0**
(site adapted)	rRMSD (%)	2.5	2.8	2.9	3.2	3.3	2.8	3.7	3.0	2.9	2.9	**2.8**
	KSI (Wh/m^2)	1.5	1.7	2.1	1.9	2.7	2.5	2.0	1.8	3.6	2.4	**1.9**
ESRA	rMBD (%)	−0.1	−0.2	0.1	−0.1	−0.1	−0.1	−0.1	−0.1	0.2	−0.3	**−0.1**
(adjusted T_L)	rRMSD (%)	3.2	3.6	3.5	3.4	3.7	3.4	3.8	3.7	3.6	3.4	**3.5**
	KSI (Wh/m^2)	4.2	5.6	4.9	4.6	5.1	5.1	5.2	5.6	5.7	5.4	**5.0**
measurement average (Wh/m^2)		641	632	621	610	595	621	626	629	622	640	**629**

Table 4: Performance of the McClear original model, the site-adapted McClear model and the locally adjusted ESRA model under clear-sky conditions. The last row is the measurement average of the clear-sky hours. The last column holds the weighted metrics average over sites.

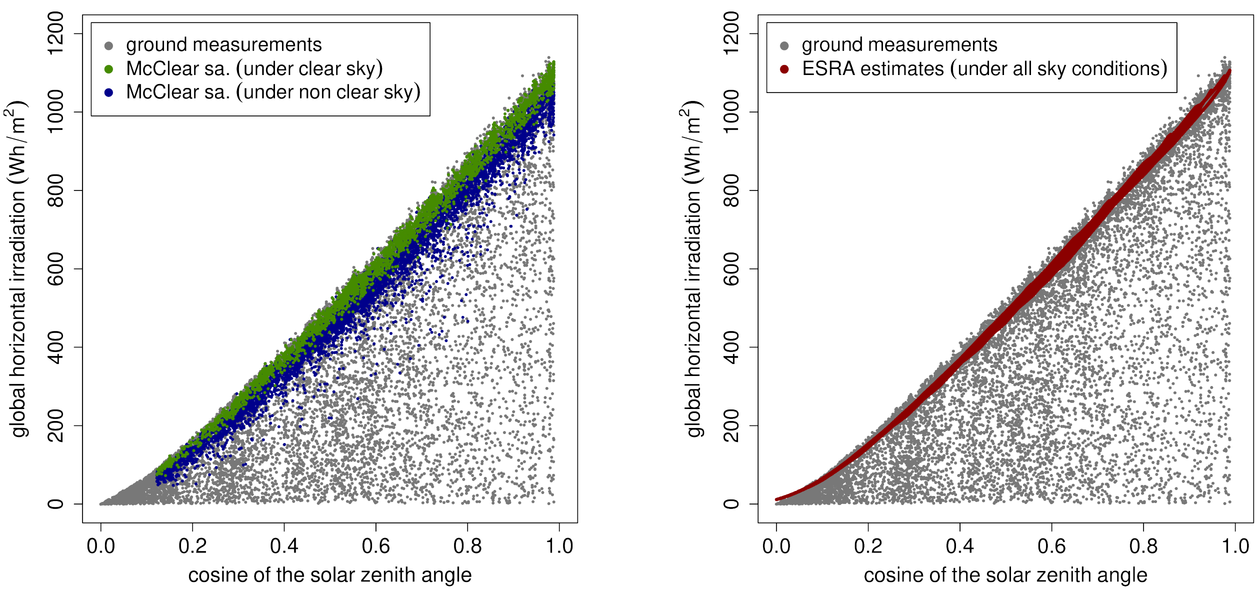

(a) Site-adapted McClear estimates under clear-sky (green) and non clear-sky (blue) conditions.

(b) Locally-adapted ESRA estimates under all-sky conditions (clear-sky and non clear-sky conditions).

Figure 6: Clear-sky estimates under different real sky conditions for McClear and ESRA models vs the cosine of the solar zenith angle. In the background, the measured ground data is in gray. For colors please refer to the online version of the manuscript.

actual water vapour content, it provides lower clear-sky estimates under cloudy sky condition than under clear-sky conditions. On the other hand, the ESRA model as implemented here is based on T_L monthly averages, so it is insensitive to short term variations in the atmosphere, in particular to the presence of clouds. This difference in the behaviour observed for these two models may appear when any model with real-time atmospheric water vapor information is compared to a model which uses average information for a given region. This issue should be taken into account in applications using clear-sky estimates under all-sky conditions.

To quantify this difference, a comparison is made between the clear-sky estimates from both models, stratified according to the actual sky condition. The average deviations (rMD) between both models are expressed according to $\Delta = \mathrm{GHI}_{\mathrm{csk}}^{\mathrm{mcclear}} - \mathrm{GHI}_{\mathrm{csk}}^{\mathrm{esra}}$, as the ESRA model estimates are not affected by the presence of clouds and thus it is more similar to a fixed upper limit for hourly all-sky conditions (see Figure 6b). The comparison between both models, shown in Table 5, has a negligible mean deviation under clear sky conditions (+0.1%, on average). However, in the presence of cloudiness, McClear estimates are systematically lower than ESRA estimates, with an average difference of −5.2%. Furthermore, negative deviations ranging between −3.9% and −6.9% are observed consistently across sites. It is important to emphasize that this analysis does not imply ranking one model over the other in terms of accuracy, but rather to highlight and quantify their different behaviour under cloudy conditions.

4.3. All-sky models (Heliosat-4, CIM)

Results for the all-sky models are presented in this Section. The evaluation includes four models: the original Heliosat-4 estimates, the site-adapted Heliosat-4 estimates and the locally adjusted CIM-ESRA and CIM-McClear models. The inclusion of the original Heliosat-4 estimates allows an evaluation of the impact of site-adaptation for this model in the region. The performance evaluation for the four all-sky models is presented in Table 6.

The original Heliosat-4 estimates have a low overall bias deviation of −0.8%, but with a variation across sites within ±1.9%. The average rRMSD metric is of 17.9%, which is to be expected for a non locally adapted and space averaged satellite based model. High dispersion across sites is also seen in the KSI metric, ranging from about 10.1 to 23.4 $\mathrm{Wh/m^2}$ with an average value of 17.7 $\mathrm{Wh/m^2}$. In the unbiased site-adapted version, the rRMSD metric is reduced only slightly to 16.8% while the KSI becomes 10.2 $\mathrm{Wh/m^2}$ (average values). The KSI is a more sensitive indicator than rRMSD and it is more reduced by the site adaptation procedure.

The locally adjusted models (CIM-ESRA and CIM-McClear) have small negative biases across all sites (negative and less than 1.4% in absolute magnitude) with a weighted average of −1.1% in both cases. This is a small but consistent underestimation observed for these models across all sites. The rRMSD metric ranges from 11.2% to 14.1% for the CIM-ESRA and from 10.6% to 13.8% for the CIM-McClear. The average rRMSD is 12.5% for CIM-ESRA and 12.1% for the CIM-McClear model. This represents a significant improvement with respect to the site-adapted Heliosat-4 estimates, whose rRMSD is in the 15.4-19.6% range, with an average of 16.8%. Similarly, the average KSI is 7.0 $\mathrm{Wh/m^2}$ for the CIM-ESRA and 8.4 $\mathrm{Wh/m^2}$ for the CIM-McClear which also represents a reduction with respect to the site-adapted Heliosat-4 (10.2 $\mathrm{Wh/m^2}$ on average). Overall, the CIMs represent a significant improvement in the accuracy of GHI estimation for this region, with respect to the Heliosat-4 method whether it is site-adapted or not. As the Heliosat-4 is a sophisticated method that considers many atmospheric inputs and phenomena, usually ranked among the best performing models, these important difference of more than

site	average of ESRA estimates ($\mathrm{Wh/m^2}$)	rMD (%) csk	rMD (%) non csk	rRMSD (%) csk	rRMSD (%) non csk	KSI ($\mathrm{Wh/m^2}$) csk	KSI ($\mathrm{Wh/m^2}$) non csk
LE	599	+0.1	−6.9	2.8	9.8	3.9	41.4
MS	608	+0.2	−4.9	2.6	7.6	5.0	29.8
LU	579	−0.1	−4.0	2.6	5.7	4.2	23.0
LB	566	+0.1	−4.2	2.8	6.5	4.6	23.8
TT	582	+0.1	−3.9	2.3	5.9	4.2	22.8
SA	589	+0.1	−5.0	2.8	7.2	5.1	29.7
RO	576	+0.1	−3.9	2.6	6.0	4.1	22.4
AR	592	+0.1	−5.8	2.8	8.4	4.9	34.4
ZU	579	−0.1	−4.9	2.8	7.7	5.2	28.4
TA	586	+0.3	−5.7	2.7	8.4	4.6	33.1
average	**592**	**+0.1**	**−5.2**	**2.7**	**7.6**	**4.4**	**30.6**

Table 5: Comparison between clear-sky models estimates: site-adapted McClear vs ESRA, under clear-sky conditions (csk) and non clear-sky conditions (non cks). The higher ESRA average is used for normalization, without implying greater accuracy. The last row shows the weighted average across sites.

4% of rRMSD metric in comparison with simple CIMs is mostly attributable to the use of the different satellite information, particularly, the different satellite FOV for the region. Local adaptation and spatial smoothing have been done to both type of models, so the difference is not attributable to these features. Heliosat-4 estimates are used here outside the recommended area and its performance is affected by the large viewing angle of the MSG satellite in the region. Hence, the difference found is a quantification of the increase in uncertainty when using CAMS all-sky GHI estimates out of the recommended area.

The CIM-McClear model has a slightly better performance than the CIM-ESRA in terms of rRMSD (12.1% compared to 12.5%). However, the opposite behavior is observed in statistical similarity, with an average KSI being 7.0 Wh/m^2 for the CIM-ESRA and 8.4 Wh/m^2 for the CIM-McClear. Therefore, it can be concluded that both CIMs have a remarkable good performance in this region and both can be used with low uncertainty for solar resource assessment. However, if these metrics are prioritized in the presented order (MBD, RMSD and KSI), the CIM-McClear model performs slightly better, as it has a similar bias but a reduced RMSD in comparison with CIM-ESRA.

The scatter plots in Figure 7 compare the three locally adapted all-sky models with the ground measurements for all sites data. The smaller dispersion of the two CIMs can be seen with the naked eye. At higher irradiances (GHI $>$ 800 Wh/m^2) an overestimation is apparent in the site-adapted Heliosat-4 estimates. For the same con-

model	metric	LE	MS	LU	LB	TT	SA	RO	AR	ZU	TA	all sites
Heliosat-4	rMBD (%)	-1.0	0.6	-3.1	-1.5	0.8	-2.6	2.6	0.2	0.6	1.9	**−0.8**
(original)	rRMSD (%)	17.5	19.4	16.6	17.3	17.8	18.0	20.4	16.8	17.7	17.7	**17.9**
	KSI (Wh/m^2)	22.0	12.8	21.3	16.0	10.1	23.4	11.2	13.6	13.9	12.5	**17.7**
Heliosat-4	rMBD (%)	0.0	0.0	0.0	0.0	0.0	0.0	0.0	0.0	0.0	0.0	**0.0**
(site adapted)	rRMSD (%)	16.0	18.6	15.4	16.4	17.3	16.5	19.6	16.0	16.9	17.0	**16.8**
	KSI (Wh/m^2)	9.5	11.6	10.3	9.5	10.1	9.0	10.6	9.7	8.8	9.0	**10.2**
CIM-ESRA	rMBD (%)	−0.9	−0.9	−1.2	−1.1	−1.2	−1.1	−1.3	−1.1	−1.1	−1.3	**−1.0**
(adjusted T_L)	rRMSD (%)	11.2	14.1	12.3	12.2	13.1	11.8	13.6	11.4	11.9	12.0	**12.5**
	KSI (Wh/m^2)	5.1	6.3	9.3	7.8	9.0	6.5	8.9	6.2	6.6	6.7	**7.0**
CIM-McClear	rMBD (%)	−0.6	−1.2	−1.3	−1.1	−1.3	−1.1	−1.4	−1.0	−1.2	−1.0	**−1.1**
(site adapted)	rRMSD(%)	10.6	13.8	12.1	12.0	12.9	11.3	13.6	11.0	11.5	11.6	**12.1**
	KSI (Wh/m^2)	4.9	9.2	10.8	8.7	10.7	7.9	10.7	7.2	8.5	7.0	**8.4**
measurement average (Wh/m^2)		463	446	465	438	437	469	427	458	440	438	**448**

Table 6: Performance metrics for the all-sky models against ground measurements: original Heliosat-4, site-adapted Heliosat-4, CIM based on ESRA and CIM based on site-adapted McClear. The last column shows the weighted average across sites.

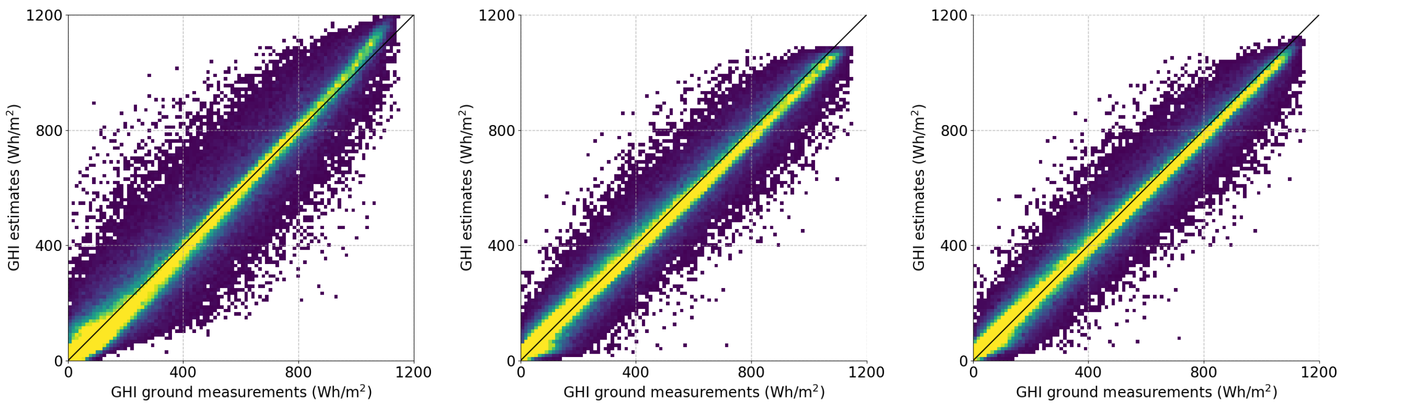

(a) Heliosat4. (b) CIM-ESRA. (c) CIM-McClear.

Figure 7: Estimates vs ground measurements for the site adapted Heliosat-4 (left), and the cloud index models based on ESRA (center) and the site adapted McClear (right) for all sites. The colour scale indicate the concentration of the samples in the scatter plot.

ditions, a small underestimation bias is observed in both CIMs. Also, a different behaviour is observed at low irradiation between the site-adapted and the locally adjusted models, with a small overestimation tendency for the former. For high irradiation values, the CIM-ESRA model present limitations, as it can be seen in the upper right side of Figure 7b. This is a consequence of using the ESRA clear-sky model as basis with an average yearly T_L cycle.

To throw some light on the specific shortcomings of each model under the different conditions, their performance indicators are discriminated by clearness index, $k_T = \mathrm{GHI}/\mathrm{GHI_o}$ (where $\mathrm{GHI_o}$ is the extraterrestrial solar irradiation at a horizontal plane at the top of the atmosphere) and by the cosine of the solar zenith angle, $\cos\theta_z$ (Iqbal, 1983). The resulting diagrams help to visualize the distribution of the deviations in terms of sun elevation and cloudiness condition. Figure 8 shows the rMBD and rRMSD diagrams for the site-adapted Heliosat-4 and the CIM-McClear at the LE site. The corresponding diagrams for the original Heliosat-4 and CIM-ESRA estimates are similar and are omitted for brevity. The comparison is intended to compare the deviations of locally adapted models that have a different nature and use different satellite inputs. Upon inspection of this figure, the metrics' patterns observed are different, and a better performance across all-sky conditions is evident for the CIM-McClear model. The rMBD of this model remains small for all the conditions (between $\simeq \pm 8\%$) and the higher deviations (rRMSD $\simeq$ 20-25%) occur around solar noon for partial cloudiness conditions (intermediate k_T values). The small overall underestimation bias observed in the model can be associated to clear-sky conditions and, to a minor extent, to cloudy conditions close to solar noon (see Figure 8b). When the Sun is low, the discriminated performance of both Heliosat-4 and CIMs are similar (low rMBD and rRMSD) for all cloudiness condition. However, when the Sun is high, the behavior changes, and errors associated to clouds are much higher for the Heliosat-4 method (see for instance, the $\simeq +40\%$ rMBD observed under this condition for this model). In fact, the rRMSD for cloudy condition ($k_T < 0.4$) at high Sun's elevation angle ($\cos\theta_z > 0.8$) are around 35-50% for Heliosat-4 and around 10-25% for the CIMs. This different behavior is related to the satellites' FOV: under this condition the optical path of the MSG satellite observation differs strongly from the optical path of the solar radiation through the atmosphere, which is not the case for the GOES-East satellite observation. In particular, midday clouds are worse perceived by the MSG satellite, resulting in higher overestimation (positive bias) and uncertainty (higher rRMSD) for the Heliosat-4. Further, as these higher deviations occur at midday when solar applications produce the most, they have an important impact in solar yield assessments. Based on this, it is clear that GOES-East satellite imagery, which has a smaller viewing angle for the region, is a better choice for local solar resource assessment.

The performance observed for the original Heliosat-4 GHI estimates is consistent with those found in the literature about the Heliosat family (Rigollier et al., 2004; Eissa et al., 2012; Ineichen, 2014; Eissa et al., 2015a; Qu et al., 2017) and it is between the expected uncertainty range for satellite-based models (Perez et al., 2013). As an example, in Ineichen (2014) a long term (8-years) uncertainty evaluation of the Heliosat-3 model (among other satellite-based models) was reported over 18 high quality measurement sites in Europe. A negligible bias and an rRMSD of 20% was found for the hourly estimates. The evaluations reported in the literature use the single pixel approach, so the hourly uncertainty showed here is lower due to the spatial smoothing. Also, most evaluations do not report the uncertainty of site-adapted versions. As mentioned previously, the evaluation of the Heliosat-4 method (not site adapted) on a hourly basis is provided by the CAMS website for several sites across the world. Two of these sites are close to the region (Buenos Aires and Florianópolis) but not representative of the broader Pampa Húmeda area. Reported rMBD for these sites are between -5-0% and the rRMSD values are between 25-28%. The biases reported in this work for the original Heliosat-4 method are in the same range, being the maximum overestimation $+11.1$ Wh/m^2 or $+2.6\%$ (for the oceanic RO site) and the maximum underestimation of -14.4 Wh/m^2 or -3.1% (at the LU site). The average RMSD found here for the Pampa Húmeda region is significantly lower, but considering spatial smoothing, and is of 80.2 Wh/m^2 or 17.9%. Site adaptation reduces slightly the RMSD to 75.2 Wh/m^2 or 16.8%. The value of the site-adaptation procedure for the region is quantified in a 1.1% reduction in rRMSD, which is significant, but not enough to achieve the reduced rRMSDs of 12-13% of the CIMs presented here due to the lower GOES-East satellite FOV in the region.

The JPT and BDJPT empirical models have been adjusted and evaluated for the same region in Alonso-Suárez et al. (2012), using GOES-East satellite images with the same spatial smoothing as here. In that work, 3 stations are used for models adjustment (LE, TT and LB) and 4 stations are used for validation. None of the validation sites is any of the sites used in this work. At the hourly level, a small overestimating bias of +1.4% and +1.1% was obtained for each model, respectively. In terms of RMSD and KSI, the overall results for the JPT model (rRMSD = 18.6% and KSI = 16 Wh/m^2) are similar to those of the original Heliosat-4 (being the former locally adjusted) and the results for the BD-JPT model (rRMSD = 14.0% and KSI = 10 Wh/m^2) are slightly above those of the CIMs considered here. Further performance evaluations between these models (using the same data set) are required, in order to have a fair comparison between alternative models for this region. However, this is not under the scope of the present work.

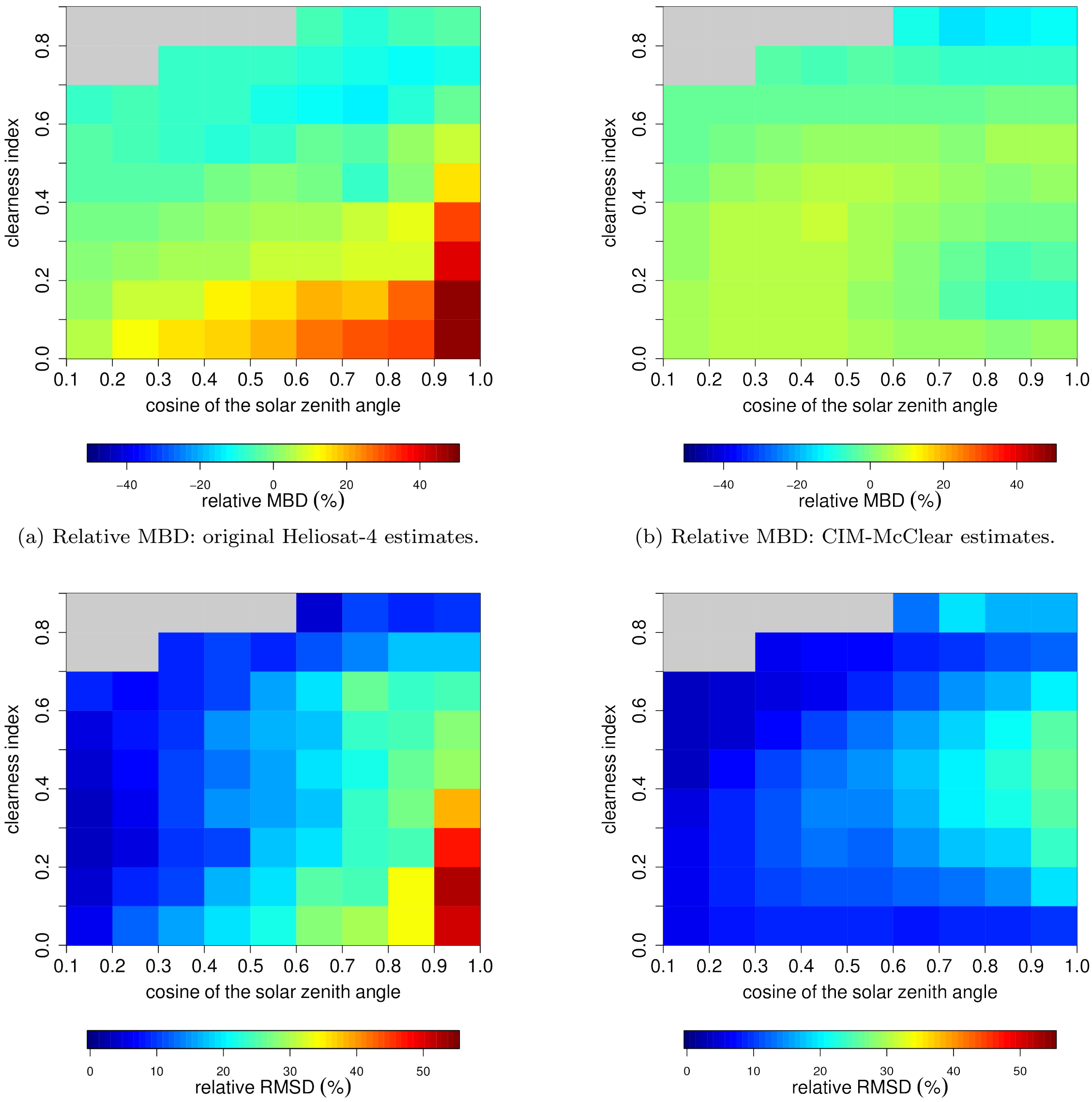

(a) Relative MBD: original Heliosat-4 estimates.

(b) Relative MBD: CIM-McClear estimates.

(c) Relative RMSD: original Heliosat-4 estimates.

(d) Relative RMSD: CIM-McClear estimates.

Figure 8: Performance metrics for the LE site discriminated by clearness index k_T and the cosine of the solar zenith angle for the site-adapted Heliosat-4 and the CIM-McClear estimates. The gray cells represent the absence of data for that condition. The values are relative to the measurements mean.

5. Conclusions

Different types of satellite-based models for estimating ground level solar global horizontal irradiation have been assessed at the hourly level using good quality ground data from 10 sites in the southeastern part of South America (Pampa Húmeda region). This region has simultaneous geostationary satellite coverage from the Meteosat Second Generation (MSG) and from the GOES-East satellites, with significantly different view angles over the area and thus provides an opportunity to quantify the effect of large view angles on the quality of the estimates.

The McClear and ESRA models have been considered for clear-sky estimation in the area. McClear estimates have been compared to clear-sky ground data with and without site-adaptation. The ESRA clear-sky model has been implemented using a daily Linke turbidity cycle which captures the average seasonal trends of the local atmosphere (this model does not use satellite information). When compared to hourly clear-sky ground data both show a similar performance, with small biases and rRMSDs in the range $\simeq 3\%$ - 4% of the measurement's average, which is similar to the ground measurement's uncertainty. McClear (even without site-adaptation) performs slightly better than the ESRA clear-sky model, due to its capacity to model the detailed atmospheric conditions on a daily basis. The site-adapted version of McClear performs best, resulting in unbiased estimates with 2.8% of rRMSD. However, the gain obtained from site-adaptation is small, 0.4% of rRMSD. To resolve between higher accurate clear-sky estimates requires pyrheliometer ground data accurate to 1% and is left for future work.

The estimates from these clear-sky models have also been compared (one to the other) under all-sky conditions of the real atmosphere, which is uncommon in clear-sky models assessments. This comparison revealed a significantly different behavior of both models: when clouds are present in the real atmosphere, McClear estimates are systematically lower than ESRA's. This is best quantified by the mean deviation between both estimates, which is 0.1% for clear-sky conditions and becomes -5.2% in the presence of clouds (i.e. McClear estimates are about 5% lower than ESRA's). This different behaviour is due to the fact that McClear is sensitive to the short-term atmospheric variability (in particular, regarding water vapor content), while our implementation of ESRA is not. Since both are commonly used clear-sky models, this may be relevant information for CIM-based all-sky models, short-term forecasting, automated quality control or other applications that make use of a clear-sky index.

For all-sky conditions, the Heliosat-4 (HS4) method and two CIMs (cloud index methods) have been considered. A first representative assessment of the HS4 method for the Pampa Húmeda region is provided, with and without site-adaptation. This model is based on the McClear clear-sky model and MSG images. The two CIMs share the same formulation for the locally adapted cloud attenuation factor based on the cloud index derived from GOES-East satellite information. One of them (CIM-ESRA) is based on the ESRA clear-sky model and the other (CIM-McClear) on the site-adapted McClear model. The major difference in the satellite images used by both approaches is the satellite view angle over the region. Similar spatial smoothing and local-adaptation are applied to both, by different means.

The HS4 estimates as provided by the CAMS-SoDa platform have the expected performance for a model without local adaptation but with spatial smoothing, showing small bias and rRMSDs in the range 16.6% - 20.4% (average 17.9%) across stations. The site-adapted version of HS4 improves slightly this performance, showing no bias and rRMSD between 15.4% and 19.6% (average 16.8%). The overall gain in rRMSD due to site-adaptation is 1.1% under all-sky conditions. The implemented CIMs exhibit a small but consistent negative bias of about -1%, so a site-adaptation post-processing can be of practical relevance for these estimates. The rRMSD is in the range 10.6% - 13.6% for CIM-McClear and 11.2% - 13.6% for CIM-ESRA. CIM-McClear has slightly smaller rRMSDs than CIM-ESRA, with averages of 12.1% for the former and 12.5% for the latter. These results for the locally adjusted CIMs are comparable to the best results found in the literature and similar to those found for an empirical model optimized for Uruguay's territory (BD-JPT model). However, the empirical nature of this model implies that its generalization to all the Pampa Húmeda area or other areas of the continent is not straightforward, since its coefficients present more spatial variability than the parameters used for local adaptation in this work. These CIMs represent a significant improvement for satellite-based solar resource assessment over the extended region.

This all-sky assessment implies that the satellite view angle over the area must be taken into account when estimating ground level solar irradiation: relatively simple CIMs using lower view angle satellite information outperform the sophisticated Heliosat-4 method which uses detailed atmospheric information and radiative transfer calculations. The MSG satellite views the region with a view angle of approximately 70°, while the GOES-East satellite has a viewing angle over this area of about 40°. It is shown that the impact of using satellite-based estimation out of the recommended area (satellite zenith angle larger than 60°) can easily account for the performance difference between MSG-based and GOES-based models observed over this region. For low solar altitude, both CIMs and HS4 present similar uncertainty for all cloudiness conditions. However, for high solar altitude, when the radiation optical path in the atmosphere is similar to that of the GOES-East but very different to that of the MSG, significantly higher errors can be observed for the HS4 model especially when partial cloudiness is present. Hence the performance difference is mostly explained by the satellites' cloud perception when the Sun is close to the zenith, which is directly related to each satellite FOV. The performance difference presented here should be read as an example of impact assessment of using solar satellite estimates out of the recommended area and is not a statement about the relative quality of the models.

In sum, the site adapted McClear clear-sky model is highly accurate in this region, but caution should be taken when using its estimates under all-sky conditions because it is sensitive to changes in atmospheric conditions under cloudy conditions. The ESRA model with local average T_L trends also gives good results for the region and it is insensitive to the presence of cloudiness in the real atmosphere. For all-sky estimates, it is not recommended to use MSG-based models over this area (even with site adaptation), due to the higher view angle and the associated decrease in accuracy. Both CIMs, based on GOES-East satellite images show a remarkable performance over this region, provide accurate hourly estimates for global solar irradiance and have the potential to be extended to a broader area. Furthermore, they can potentially be adapted to provide DNI estimates or, combined with spectral clear-sky models, provide spectral estimates for global irradiation.

Acknowledgments

The authors thank R. Righini and R. Aristegui from GERSOLAR/UNLU (Argentina) for providing us with the ground data for the Luján site and the SONDA network of the INPE (Brazil) for providing the São Martinho da Serra data set. The authors acknowledge financial support from the ANII-FSE-110011 grant of the Uruguay's National Research and Innovation Agency (ANII) and also from CSIC UDELAR (Uruguay) under proyect 2019-117.

References

Abal, G., Aicardi, D., Alonso-Suárez, R., & Laguarda, A. (2017). Performance of empirical models for diffuse fraction in Uruguay. *Solar Energy*, *141*, 166–181. doi:10.1016/j.solener.2016.11.030.

Alonso-Suárez, R. (2017). *Estimación del recurso solar en Uruguay mediante imágenes satelitales*. Ph.D. thesis Facultad de Ingeniería, Universidad de la República. Available at: https://hdl.handle.net/20.500.12008/20200.

Alonso-Suárez, R., Abal, G., Musé, P., & Siri, R. (2014). Satellite-derived solar irradiation map for Uruguay. In *Elsevier Energy Procedia* (pp. 1237–1246). volume 57. doi:10.1016/j.egypro.2014.10.072.

Alonso-Suárez, R., Abal, G., Siri, R., & Musé, P. (2012). Brightness-dependent Tarpley model for global solar radiation estimation using GOES satellite images: application to Uruguay. *Solar Energy*, *86*, 3205–3215. doi:10.1016/j.solener.2012.08.012.

Antonanzas-Torres, F., Urraca, R., Polo, J., nán Lamigueiro, O. P., & Escobar, R. (2019). Clear sky solar irradiance models: A review of seventy models. *Renewable and Sustainable Energy Reviews*, *107*, 374–387. doi:10.1016/j.rser.2019.02.032.

Beyer, G. B., Costanzo, C., & Heinemann, D. (1996). Modifications of the heliosat procedure for irradiance estimates from satellite images. *Solar Energy*, *56*, 207–212. doi:10.1016/0038-092X(95)00092-6.

Cano, D., Monget, J., Albuisson, M., Guillard, H., Regas, N., & Wald, L. (1986). A method for the determination of the global solar radiation from meteorological satellite data. *Solar Energy*, *37*, 31–39. doi:10.1016/0038-092X(86)90104-0.

Ceballos, J. C., Bottino, M., & de Souza, J. (2004). A simplified physical model for assessing solar radiation over Brazil using GOES 8 visible imagery. *Journal of Geophysical Research: Atmospheres*, *109*. doi:10.1029/2003JD003531.

Cebecauer, T., Suri, M., & Perez, R. (2010). High performance MSG satellite model for operational solar energy applications. In *Proceedings of the American Solar Energy Society (ASES)* (pp. 1–5). Phoenix, Arizona, United States.

Eissa, Y., Chiesa, M., & Ghedira, H. (2012). Assessment and recalibration of the Heliosat-2 method in global horizontal irradiance modeling over the desert environment of the UAE. *Solar Energy*, *86*, 1816–1825. doi:10.1016/j.solener.2012.03.005.

Eissa, Y., Korany, M., Aoun, Y., Boraiy, M., Abdel Wahab, M. M., Alfaro, S. C., Blanc, P., El-Metwally, M., Ghedira, H., Hungershoefer, K., & Wald, L. (2015a). Validation of the surface downwelling solar irradiance estimates of the HelioClim-3 database in Egypt. *Remote Sensing*, *7*, 9269–9291. doi:10.3390/rs70709269.

Eissa, Y. E., Munawwar, S., Oumbe, A., Blanc, P., Ghedira, H., Wald, L., Bru, H., & Goffe, D. (2015b). Validating surface downwelling solar irradiances estimated by the mcclear model under cloud-free skies in the United Arab Emirates. *Solar Energy*, (pp. 17–31). doi:10.1016/j.solener.2015.01.017.

Engerer, N., & Mills, F. (2015). Validating nine clear sky radiation models in Australia. *Solar Energy*, *120*, 9–24. doi:10.1016/j.solener.2015.06.044.

Espinar, B., Ramírez, L., Drews, A., Beyer, H. G., Zarzalejo, L. F., Polo, J., & Martín, L. (2009). Analysis of different comparison parameters applied to solar radiation data from satellite and german radiometric stations. *Solar Energy*, *83*, 118–125. doi:10.1016/j.solener.2008.07.009.

Gueymard, C. A. (2008). Rest2: High-performance solar radiation model for cloudless-sky irradiance, illuminance, and photosynthetically active radiation – validation with a benchmark dataset. *Solar Energy*, *82*, 272–285. doi:10.1016/j.solener.2007.04.008.

Gueymard, C. A. (2012). Clear-sky irradiance predictions for solar resource mapping and large-scale applications: Improved validation methodology and detailed performance analysis of 18 broadband radiative models. *Solar Energy*, *86*, 2145–2169. doi:10.1016/j.solener.2011.11.011. Progress in Solar Energy 3.

Gueymard, C. A. (2014). A review of validation methodologies and statistical performance indicators for modeled solar radiation data: Towards a better bankability of solar projects. *Renewable and Sustainable Energy Reviews*, *39*, 1024–1034. doi:10.1016/j.rser.2014.07.117.

Ineichen, P. (2014). Long term satellite global, beam and diffuse irradiance validation. *Energy Procedia*, *48*, 1586–1596. doi:10.1016/j.egypro.2014.02.179. Proceedings of the 2nd International Conference on Solar Heating and Cooling for Buildings and Industry (SHC 2013).

Ineichen, P. (2016). Validation of models that estimate the clear sky global and beam solar irradiance. *Solar Energy*, *132*, 332–344. doi:10.1016/j.solener.2016.03.017.

Ineichen, P., & Perez, R. (2002). A new airmass independent formulation for the Linke turbidity coefficient. *Solar Energy*, *73*, 151–157. doi:10.1016/S0038-092X(02)00045-2.

Iqbal, M. (1983). *An introduction to solar radiation*. Academic Press.

Johnson, D. B., Flament, P., & Bernstein, R. L. (1994). High-resolution satellite imagery for mesoscale meteorological studies. *Bulletin of the American Meteorological Society*, *75*, 5–34. doi:10.1175/1520-0477(1994)075<0005:HRSIFM>2.0.CO;2.

Justus, C., Paris, M., & Tarpley, J. (1986). Satellite-measured insolation in the United States, Mexico, and South America. *Remote Sensing of Environment*, *20*, 57–83. doi:10.1016/0034-4257(86)90014-3.

Kriebel, K., Gesell, G., Kästner, M., & Mannstein, H. (2003). The cloud analysis tool APOLLO: Improvements and validations. *International Journal of Remote Sensing*, *24*, 2389–2408. doi:10.1080/01431160210163065.

Kriebel, K., Saunders, R., & Gesell, G. (1989). Optical properties of clouds derived from fully cloudy AVHRR pixels. *Beiträge zur Physik der Atmosphäre*, *62*, 165–171.

Laguarda, A., & Abal, G. (2016). Índice de turbidez de Linke a partir de irradiación solar global en Uruguay. *Avances en Energías Renovables y Medio Ambiente*, *20*, 11.35–11.46.

Laguarda, A., & Abal, G. (2017). Clear-Sky broadband irradiance: first model assessment in Uruguay. In *ISES Conference Proceedings, Solar World Congress 2017* Solar Radiation Availability and Variability (pp. 1–12).

Laguarda, A., Alonso-Suárez, R., & Abal, G. (2018). Modelo semi-empírico de irradiación solar global a partir de imágenes satelitales GOES. In *Anais do VII Congresso Brasileiro de Energia Solar 2018* Radiação Solar (pp. 1–9).

Lefevre, M., & Wald, L. (2016). Validation of the mcclear clear-sky model in desert conditions with three stations in Israel. *Adv. Sci. Res*, *13*, 21–26. doi:10.5194/asr-13-21-2016.

Lefèvre, M. (2018). *Regular Validation Report*. Technical Report D72.1.3.1 Copernicus Atmosphere Monitoring Service. URL: https://atmosphere.copernicus.eu/sites/default/files/2019-06/23_CAMS72_2018SC1_D72.1.3.1-JJA2018_RAD_validation_report-201903_v3.pdf.

Lefèvre, M., Oumbe, A., Blanc, P., Espinar, B., Qu, Z., Wald, L., Homscheidt, M. S., & Arola, A. (2013). McClear: a new model estimating downwelling solar radiation at ground level in clear-sky conditions. *Atmospheric Measurement Techniques, European Geosciences Union*, *6*, 2403–2418. doi:10.5194/amt-6-2403-2013.

Linke, F. (1922). Transmissions-koeffizient und trubungsfaktor. *Meteoreorological Magazine Beitraege zur Physik der Atmosphaere-Beitr*, *10*, 91–103.

Lockheed-Martin (2019). *GOES-R series data book*. Technical Report Contract NNG09HR00C National Aeronautics and Space Administration.

Massey Jr., F. J. (1951). The Kolmogorov-Smirnov test for goodness of fit. *Journal of the American Statistical Association*, *46*, 68–78.

Mayer, B., & Kylling, A. (2005). Technical note: The libRadtran software package for radiative transfer calculations – description and examples of use. *Atmospheric Chemistry and Physics*, *5*, 1855–1877.

McArthur, L. (2005). *Baseline Surface Radiation Network Operations Manual*. Technical Report WCRP-121/ WMO TD-No. 1274 World Climate Research Programme – WMO.

Peel, M. C., Finlayson, B. L., & Mcmahon, T. A. (2007). Updated world map of the köppen-geiger climate classification. *Hydrology and Earth System Sciences Discussions*, *11*, 1633–1644.

Perez, R., Cebecauer, T., & Suri, M. (2013). Chapter 2 - semi-empirical satellite models. In J. Kleissl (Ed.), *Solar Energy Forecasting and Resource Assessment* (pp. 21–48). Boston: Academic Press. doi:10.1016/B978-0-12-397177-7.00002-4.

Perez, R., Ineichen, P., Moore, K., Kmiecik, M., Chain, C., George, R., & Vignola, F. (2002). A new operational model for satellite-derived irradiances: description and validation. *Solar Energy*, *73*, 307–317. doi:10.1016/S0038-092X(02)00122-6.

Perez, R., Ineichen, P., Seals, R., & Zelenka, A. (1990). Making full use of the clearness index for parameterizing hourly insolation conditions. *Solar Energy*, *45*, 111–114. doi:10.1016/0038-092X(90)90036-C.

Polo, J., Wilbert, S., Ruiz-Arias, J., Meyer, R., Gueymard, C., Súri, M., Martín, L., Mieslinger, T., Blanc, P., Grant, I., Boland, J., Ineichen, P., Remund, J., Escobar, R., Troccoli, A., Sengupta, M., Nielsen, K., Renne, D., Geuder, N., & Cebecauer, T. (2016). Preliminary survey on site-adaptation techniques for satellite-derived and reanalysis solar radiation datasets. *Solar Energy*, *132*, 25–37. doi:10.1016/j.solener.2016.03.001.

Qu, Z. (2013). *La nouvelle méthode Heliosat-4 pour l'évaluation du rayonnement solaire au sol*. Ph.D. thesis L'École nationale supérieure des mines de Paris. Available at: https://pastel.archives-ouvertes.fr/pastel-00957358/file/2013ENMP0040.pdf.

Qu, Z., Oumbe, A., Blanc, P., Espinar, B., Gesell, G., Gschwind, B., Klüser, L., Lefèvre, M., Saboret, L., Schroedter-Homscheidt, M., & Wald, L. (2017). Fast radiative transfer parameterisation for assessing the surface solar irradiance: The Heliosat-4 method. *Meteorologische Zeitschrift*, *26*, 33–57. doi:10.1127/metz/2016/0781.

Remund, J., Wald, L., Lefevre, M., Ranchin, T., & Page, J. (2003). Worldwide Linke turbidity information. In *Proceedings of ISES Solar World Congress*. URL: https://hal.archives-ouvertes.fr/hal-00465791/file/ises2003_linke.pdf.

Rigollier, C., Bauer, O., & Wald, L. (2000). On the clear sky model of the ESRA – European Solar Radiation Atlas – with respect to the Heliosat method. *Solar Energy*, *68*, 33–48. doi:10.1016/S0038-092X(99)00055-9.

Rigollier, C., Lefevre, M., & Wald, L. (2004). The method Heliosat-2 for deriving shortwave solar radiation from satellite images. *Solar Energy*, *77*, 159–169. doi:10.1016/j.solener.2004.04.017.

Ruiz-Arias, J. A., & Gueymard, C. A. (2018). A multi-model benchmarking of direct and global clear-sky solar irradiance predictions at arid sites using a reference physical radiative transfer model. *Solar Energy*, *171*, 447–465. doi:10.1016/j.solener.2018.06.048.

Schroedter-Homscheidt, M., Hoyer-Klick, C., Killius, N., Betcke, J., Lefevre, M., Wald, L., Wey, E., & Saboret, L. (2018). *User's Guide to the CAMS Radiation Service*. Technical Report Copernicus Atmosphere Monitoring Service.

Dias da Silva, P. E., Martins, F. R., & Pereira, E. B. (2014). Quality control of solar radiation data within SONDA network in Brazil: preliminary results. In *ISES Conference Proceedings, EuroSun 2014* Solar Radiation Availability and Variability (pp. 1–9). doi:10.18086/eurosun.2014.08.04.

Sun, X., Bright, J. M., Gueymard, C. A., Acord, B., Wang, P., & Engerer, N. A. (2019). Worldwide performance assessment of 75 global clear-sky irradiance models using principal component analysis. *Renewable and Sustainable Energy Reviews*, *111*, 550–570. URL: http://www.sciencedirect.com/science/article/pii/S1364032119302187. doi:https://doi.org/10.1016/j.rser.2019.04.006.

Tarpley, J. (1979). Estimating incident solar radiation at the surface from geostationary satellite data. *Journal of Applied Meteorology*, *18*, 1172–1181. doi:10.1175/1520-0450(1979)018<1172:EISRAT>2.0.CO;2.

WDC (2015). Cloud physical parameters from SEVIRI at WDC-RSAT. URL: http://wdc.dlr.de/data_products/CLOUDS/clouds_seviri.php.